Journal of Alloys and Compounds 507 (2010) 167–171

Contents lists available at ScienceDirect

Journal of Alloys and Compounds

journal homepage: www.elsevier.com/locate/jallcom

Fabrication of Ag–Sn–Sb–Te based thermoelectric materials by MA-PAS and their properties

Jin Wu, Junyou Yang*, Hui Zhang, Jiansheng Zhang, Shuanglong Feng, Ming Liu, Jiangying Peng, Wen zhu, Tao Zou

State Key Laboratory of Material Processing and Die & Mould Technology, Huazhong University of Science and Technology, Wuhan 430074, PR China

ARTICLE INFO

Article history:
Received 18 June 2010
Received in revised form 19 July 2010
Accepted 21 July 2010
Available online 29 July 2010

Keywords:
Mechanical alloying
$AgSn_{18}SbTe_{20}$
SnTe
Plasma activated sintering
Electrical properties

ABSTRACT

Starting from elemental powder mixtures of $AgSn_{18}SbTe_{20}$ and $Sn_{50}Te_{50}$, P-type $AgSn_{18}SbTe_{20}$ and $Sn_{50}Te_{50}$ bulk thermoelectric materials were fabricated by a combined process of mechanical alloying (MA) and plasma activated sintering (PAS). It was found that SnTe compound could be easily synthesized after milling only for 1 h. Prolonging the milling time, Ag and Sb atoms diffused into the lattice of the primary SnTe compound gradually and SnTe-based solid solution was formed. The electrical resistivity and Seebeck coefficient of the as-PASed samples were measured from 323 K to 723 K. The maximum power factor of 1.98×10^{-3} Wm^{-1} K^{-2} was obtained at 673 K for $AgSn_{18}SbTe_{20}$ and it was higher than that of the material with similar composition from previous published literature.

1. Introduction

Due to the worldwide energy shortage and environment problem, thermoelectric materials reattract much attention and get reflourishing in recent years. Currently the main problem for thermoelectric materials is their low efficiency, and the figure of merit (ZT) of traditional thermoelectric materials is about one unity [1–6], which is too low to afford a large scale application. Recently a new material of $AgPb_mSbTe_{m+2}$ named as LAST had been reported by Hsu et al. [6], and an extraordinary high thermoelectric performance of ZT = 2.2 was obtained at 800 K for this material [7]. This is also the highest ZT value that has ever been reported for bulk thermoelectric materials. Unfortunately, high Pb content in LAST is very negative to the environment, therefore, substituting Pb partially with Sn or other elements in LAST has been tried by some researchers [8–11], and good thermoelectric properties are also obtained in some systems [12–15]. However, lead-free "LAST" materials, e.g., completely replacing Pb with Sn to form a SnTe-based "LAST" structure, have less been reported. Furthermore, current preparation process for LAST materials is quite time-taking and heavily energy-consuming [7]. So it is of great significance to develop new processing methods and explore environmental-benign new composition systems for "LAST" materials.

MA-PAS, which is a combination of mechanical alloying and plasma activated sintering, has been proved to be a very effective preparation method for thermoelectric materials in our previous work [16–19]. As a part of our research work on lead-free "LAST" materials, Pb will be completely replaced with Sn in this work, and a combined process of MA-PAS will be employed to synthesize the lead-free "LAST" of $AgSn_{18}SbTe_{20}$. For comparison, $Sn_{50}Te_{50}$, which corresponds to the composition of SnTe compound, was also processed with the same procedure. The phase and microstructure evolution during the MA-PAS process and their electrical performance will be reported in the paper.

2. Experimental

Elemental powders of Te (100 mesh, >99.9 wt.%), Sb (100 mesh, 99.9 wt.%), Sn (100 mesh, >99.99 wt.%), Ag (100 mesh, >99.99 wt.%) were used as the starting materials. According to the composition formula of $AgSn_{18}SbTe_{20}$ and $Sn_{50}Te_{50}$, the powders were weighed and loaded into two stainless steel jars respectively, and then subjected to mechanical alloying in a QM-ISP4-Cl planetary ball mill. The charge had a ball-to-powder ratio of 40:1, the rotation speed was fixed at 400 rpm, and the milling atmosphere is purified argon. During the MA process, some powders were taken out in a certain interval for morphology, structure and thermal analysis. Subsequently, the as-MAed powder was consolidated at 653 K for 15 min by PAS under a pressure of 40 MPa. Seebeck coefficients (α) was measured by applying a 10 K temperature difference between the two ends of a 3 mm × 3 mm × 15 mm bar specimen and measuring the output voltage ΔV between them, and then calculating the value by $\alpha = \Delta V/\Delta T$. A four probe method was engaged for electrical resistivity measurement.

Microstructure observation was performed with a field emission scanning electron microscope (Sirion 200). Phase identification was performed with a Philips X'Pert PRO diffractometer by using Cu Kα radiation (λ = 1.5406 Å). Differential ther-

* Corresponding author. Tel.: +86 27 87558310; fax: +86 27 87558310.
E-mail address: junyou.yang@163.com (J. Yang).

0925-8388/$ – see front matter © 2010 Elsevier B.V. All rights reserved.
doi:10.1016/j.jallcom.2010.07.146

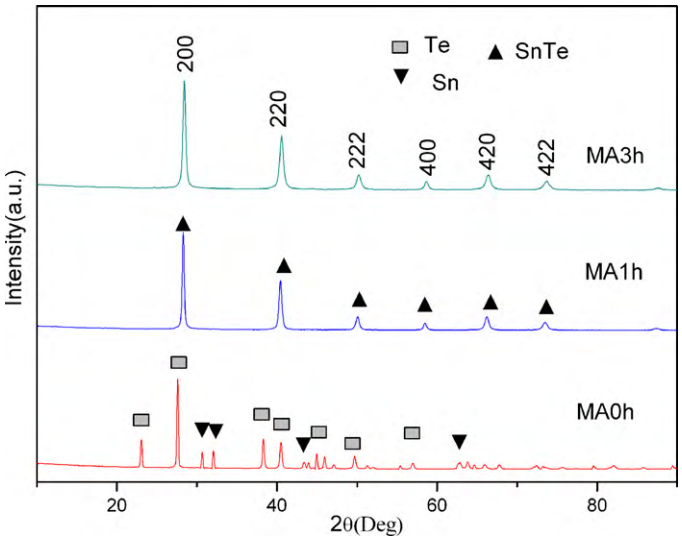

Fig. 1. XRD patterns of $Sn_{50}Te_{50}$ powders with different milling time.

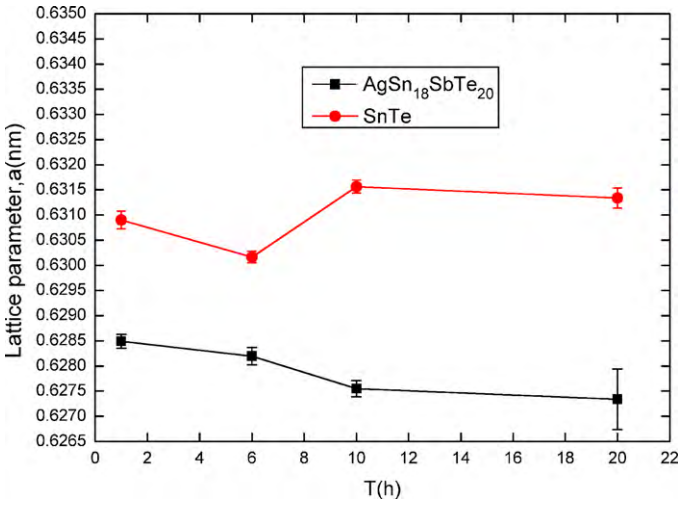

Fig. 3. Variation of lattice constants of $AgSn_{18}SbTe_{20}$ and SnTe with different milling time.

mal analysis (DTA) was performed at a heating rate of 20 °C/min with a Diamand TG/DTA6300.

3. Results and discussion

The XRD patterns of $Sn_{50}Te_{50}$ powders with different milling time were shown in Fig. 1. It can be seen that all elemental peaks of Sn and Te disappeared after MA for 1 h, the peaks of SnTe compound appeared. Further prolonging the milling time to 20 h, there was no evident change in the XRD patterns, indicating that all elemental Sn and Te powders reacted into single-phase SnTe compound after milling for 1 h.

As shown in Fig. 2, after MA for 1 h, elemental peaks of Sn and Te disappeared, and those of SnTe compound were detected. Further prolonging the milling time, no new peak appeared, while the peak intensities of SnTe compound decreased and the main peak shifted to high angle direction, indicating that a SnTe-based solid solution was formed during mechanical alloying in the $AgSn_{18}SbTe_{20}$ system. It is similar with the $AgPb_{18}SbTe_{20}$ system, which has a PbTe-based solid solution structure [1]. Fig. 2 also shows the XRD pattern of the as-PASed $AgSn_{18}SbTe_{20}$ bulk sample, which has almost the same XRD pattern as the MA-derived powders.

The lattice constants of the SnTe compound and the SnTe-based solid solution, which were calculated with the least square method from the XRD data of Figs. 1 and 2 respectively, are shown in Fig. 3. It demonstrates that the lattice constant of the SnTe compound is larger than that of the SnTe-based solid solution. This can be attributed to the substitution of Ag and Sb atoms for Sn atoms in the SnTe-based solid solution of $AgSn_{18}SbTe_{20}$. Considering that the atomic radius of Sb (1.4 Å) is smaller than that of Sn (1.72 Å), and the atomic radius of Ag (1.75 Å) is close to that of Sn (1.72 Å), so the lattice constant of $AgSn_{18}SbTe_{20}$ becomes smaller after the substitution. With prolonged the milling time, the substitution content of Ag and Sb atoms for Sn increases gradually. Therefore, the lattice constant of the SnTe-based solid solution decreased with prolonged milling time.

To clarify the phase evolution during the MA process, DTA experiments were also performed and shown in Fig. 4. It can be seen that there are two endothermic peaks and one exothermic peak in the DTA curve of $AgSn_{18}SbTe_{20}$ powders before milling. Referring to the Sn–Te phase diagram [20], the first peak at 235 °C is the melt-

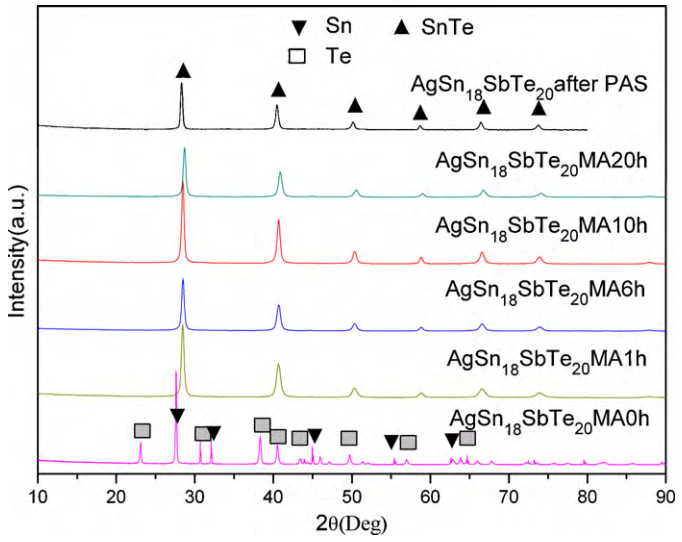

Fig. 2. XRD patterns of the as-MAed $AgSn_{18}SbTe_{20}$ powders and the as-PASed $AgSn_{18}SbTe_{20}$ bulk materials.

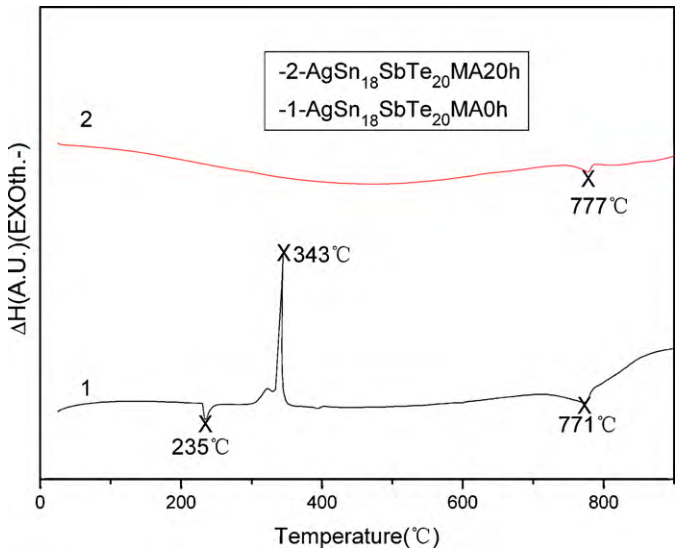

Fig. 4. DTA curves of $AgSn_{18}SbTe_{20}$ powders with different milling time.

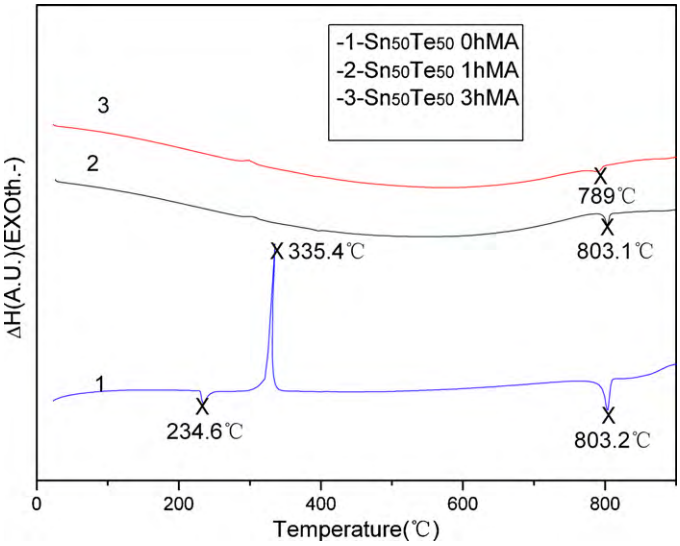

Fig. 5. DTA curves of SnTe powders with different milling time.

ing peak of Sn powders, and the second exothermic peak at 343 °C corresponds to the synthesis reaction of Te + Sn → SnTe, and the third peak at 771.1 °C is the melting peak of SnTe compound. However, there is no peak corresponding to the synthesis reaction of Te + Sn → SnTe at 343 °C in cure 2, and only one endothermic peak at 777 °C is detected in curve 2, corresponding to the melting peak of the SnTe compound, indicating that the powders milled for 20 h are a SnTe-based $AgSn_{18}SbTe_{20}$ single-phase solid solution. This is in agreement with the XRD results in Fig. 2.

The DTA curves of $Sn_{50}Te_{50}$ powders with different milling time were shown in Fig. 5 for comparison. Only one endothermic peak located at 803.1 °C, which corresponds to the melting peak of the SnTe compound, appears in the DTA curve of the powders milled for 1 h, and no elemental melting peak appears in the DTA curve of the 1 h sample, indicating that single-phase SnTe compound can be synthesized by mechanical alloying for 1 h. There is no peak corresponding to the synthesis reaction of Te + Sn → SnTe at 335.4 °C in cure 2 and cure 3, suggesting that all elemental powders of Te and Sn reacted into SnTe completely after milling for 1 h. It is in good consistence with the XRD results in Fig. 1.

SEM micrographs of $AgSn_{18}SbTe_{20}$ powders with different milling time were shown in Fig. 6 (a–d). The morphology and size of the powders are very inhomogeneous in the primary stage of MA, and the particle size ranges from 30 nm to 10 μm for the 1 h as-MAed powders. When increasing the milling time, the mean powder particle size decreases, and the powder morphology becomes more homogenous. The average particle size of $AgSn_{18}SbTe_{20}$ powders milled for 20 h is about 1 μm.

The as-MAed powders of $AgSn_{18}SbTe_{20}$ and SnTe were consolidated by plasma activated sintering. The electrical properties of as-PASed $AgSn_{18}SbTe_{20}$ and SnTe as a function of temperature were shown in Figs. 7–9. As shown in Fig. 7, the electrical conductivities of $AgSn_{18}SbTe_{20}$ and SnTe were much higher than that of $AgPb_mSbTe_{m+2}$ [6] at the same temperature, which demonstrates replacing Pb with Sn in LAST materials can greatly enhance its electrical conductivity. Both the electrical conductivities of $AgSn_{18}SbTe_{20}$ and SnTe monotonically decrease with increasing temperature, indicating of metal conductive behavior in the whole temperature range examined. The high electrical conductivity of $AgSn_{18}SbTe_{20}$, compared with that of $AgPb_mSbTe_{m+2}$ [6], is consistent with the high electrical conductivity of SnTe, which is the result of massive, naturally occurring Sn vacancies in the lattice

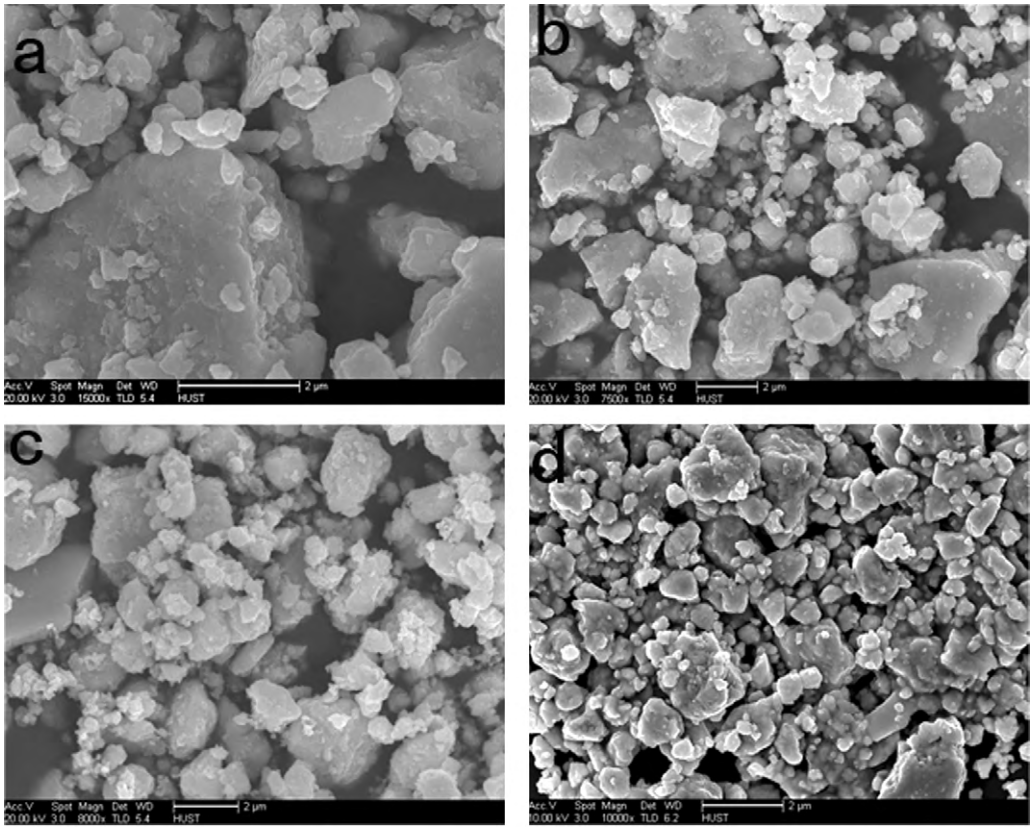

Fig. 6. SEM micrographs of $AgSn_{18}sbTe_{20}$ powders (a) milled for 1 h (b) milled for 3 h (c) milled for 6 h and (d) milled for 20 h.

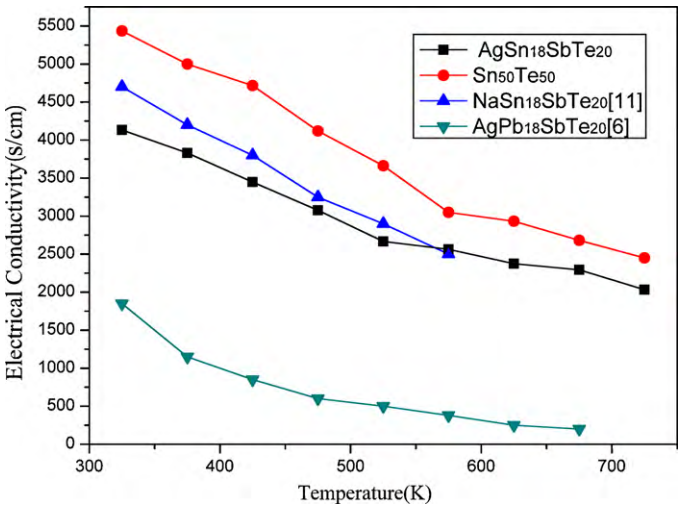

Fig. 7. Temperature dependence of the electrical conductivities of $AgSn_{18}SbTe_{20}$ and SnTe.

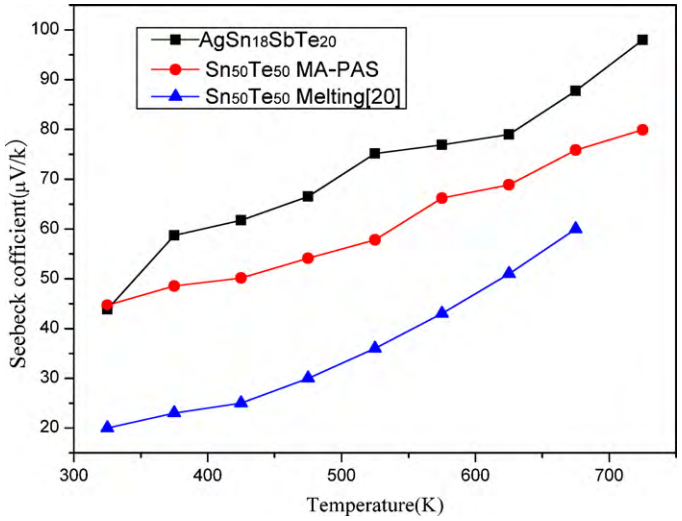

Fig. 8. Temperature dependence of the Seebeck coefficient of $AgSn_{18}SbTe_{20}$ and SnTe.

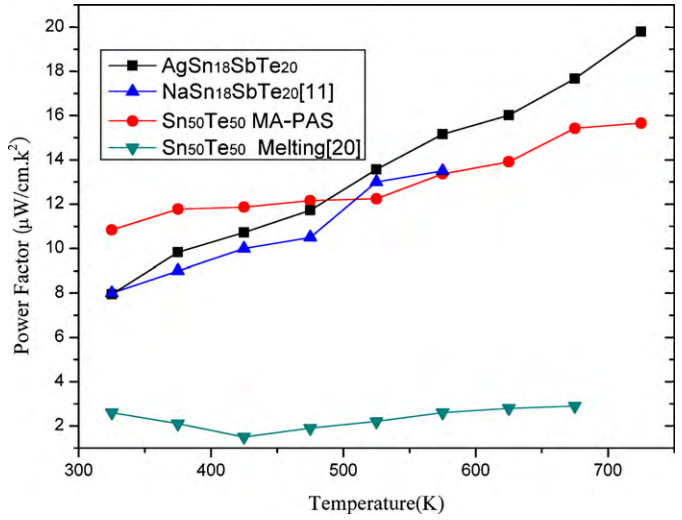

Fig. 9. Temperature dependence of the power factor of $AgSn_{18}SbTe_{20}$ and SnTe.

that strongly increases the carrier concentration [11]. Similar to the electrical conductivity of $NaSn_{18}SbTe_{20}$ [11], the electrical conductivity of $AgSn_{18}SbTe_{20}$ was also lower than that of SnTe at the same temperature, indicating that adding Ag and Sb atoms into SnTe compound was conductive to decrease the electrical conductivity of SnTe. It is likely that Ag and Sb atoms in the lattice of SnTe-based compound can increase the electrical scattering and prevent electronic conduction, therefore, the electirical conductivity of Ag and Sb codoped SnTe compound was lower than that of the undoped-SnTe compound.

As Fig. 8 shows, both $AgSn_{18}SbTe_{20}$ and SnTe compounds had a positive Seebeck coefficient in the temperature range from 323 K to 673 K, suggesting a p-type conductive behavior. The increase of Seebeck coefficient of both $AgSn_{18}SbTe_{20}$ and SnTe with increasing temperature was consistent with the increase of electrical resistivity. The Seeback coefficient of $AgSn_{18}SbTe_{20}$ and SnTe arrived 99 μV/K and 80 μV/K at 723 K, respectively, which were much higher than that of SnTe [20] prepared by other method.

As it shows in Fig. 9, both the power factors of $AgSn_{18}SbTe_{20}$ and SnTe increased with the increase of temperature. The power factor of $AgSn_{18}SbTe_{20}$ was lower than that of SnTe below 475 K, while the power factor of $AgSn_{18}SbTe_{20}$ surpassed that of SnTe when the temperature was higher than 475 K. The power factor of $AgSn_{18}SbTe_{20}$ was $1.98 \times 10^{-3}\,Wm^{-1}\,K^{-2}$ at 723 K, which was higher than those of $NaSn_{18}SbTe_{20}$ [11] and SnTe [20] reported before. This demonstrates Ag and Sb codoped SnTe compound had better thermoelectric properties than undoped-SnTe compound within some temperature range.

4. Conclusion

(1) Starting from elemental powder mixtures of $Sn_{50}Te_{50}$ and $AgSn_{18}SbTe_{20}$, SnTe compound and SnTe-based solid solution were synthesized by mechanical alloying (MA) respectively.
(2) The as-MAed $AgSn_{18}SbTe_{20}$ has a SnTe-based solid solution structure. With prolonged milling time, more and more Ag and Sb atoms enter into SnTe-based structure of $AgSn_{18}SbTe_{20}$ and substitute for Sn, so the lattice spacing of SnTe-based solid solution decreases.
(3) The P-type $AgSn_{18}SbTe_{20}$ and SnTe compounds were obtained by MA and subsequently PAS in this work. The maximum power factor of $1.98 \times 10^{-3}\,Wm^{-1}\,K^{-2}$ was obtained at 723 K for $AgSn_{18}SbTe_{20}$, which was higher than those of $NaSn_{18}SbTe_{20}$ and SnTe reported before. It also shows Ag and Sb codoped SnTe compounds had better electrical properties than undoped-SnTe compounds within some temperature range.

Acknowledgments

This work is co-financed by National Natural Science Foundation of China (No. 50827204) and the Cultivation Fund of the Key Scientific and Technical Innovation Project, Ministry of Education of China (No. 707044). The technical assistance from the Analytical and Testing Center of HUST is also gratefully acknowledged.

References

[1] M. Zhou, J.F. Li, H. Wang, Chin. Sci. Bull. 52 (2007) 990–996.
[2] M. Zhou, J.F. Li, Takuji Kita, J. Am. Chem. Soc. 130 (2008) 4527–4532.
[3] B. Poudel, Q. Hao, Y. Ma, Y.C. Lan, A. Minnich, Science 320 (2008) 634.
[4] J.P. Heremane, V. Jovovic, E. Toberer, A. Saramat, Science 321 (2008) 554.
[5] J.S. Rhyee, K.H. Lee, et al., Nature 459 (2009) 965–968.
[6] K.F. Hsu, S. Loo, F. Guo, W. Chen, Science 303 (2004) 818.
[7] H. Wang, J.F. Li, C.W. Nan, M. Zhou, Appl. Phys. Lett. 88 (2006) 092104.
[8] A. Kosuga, K. Kurosaki, H. Muta, S. Yamanaka, J. Alloys Compd. 416 (2006) 218–221.
[9] J. Androulakis, K.F. Hsu, R. Pcionek, Adv. Mater. 18 (2006) 1170–1173.
[10] J. Androulakis, R. Pcionek, E. Quarez, Chem. Mater. 18 (2006) 4719–4721.

[11] A. GuéguenA, P.F.P. Poudeu, C.P. Li, Chem. Mater. 21 (2009) 1683–1694.
[12] M.K. Han, K. Hoang, Chem. Mater. 20 (2008) 3512–3520.
[13] H. Wang, J.F. Li, M. Zou, T. Sui, Appl. Phys. Lett. 93 (2008) 202106.
[14] H. Wang, J.F. Li, T. Kita, J. Phys. D: Appl. Phys. 40 (2007) 6839–6845.
[15] P.F.P. Poudeu, J. DAngelo, H. Kong, J. Am. Chem. Soc. 128 (2006) 14347–14355.
[16] J.Y. Yang, Y.H. Chen, J. Alloys Compd. 375 (2004) 229–232.
[17] Xi'an Fan, Junyou Yang, Wen Zhu, J. Alloys Compd. 448 (2008) 308–312.
[18] Xi'an Fan, Junyou Yang, Wen Zhu, J. Alloys Compd. 420 (2006) 256–259.
[19] X.A. Fan, J.Y. Yang, R.G. Chen, J. Phys. D: Appl. Phys. 39 (2006) 740–745.
[20] Y. Gelbstein, J. Appl. Phys. 105 (2009) 023713.